micromachines

MDPI

Article

A Piezoelectric MEMS Microgripper for Arbitrary XY Trajectory

Fabio Botta

Depatment of Industrial, Electronic and Mechanical Engineering, Roma Tre University, Via Vito Volterra 62, 00146 Roma, Italy; fabio.botta@uniroma3.it; Tel.: +39-06-5733-3491

Abstract: In this paper, a piezoelectric microgripper for arbitrary 2D trajectory is proposed. The desired trajectory of the specimen under consideration was obtained by the deformability of a structure consisting of 16 straight beams and 12 C-structures. The mechanical action that deforms the structure was obtained by an electrical voltage supplied to piezoelectric plates. In order to verify the proposed model a FEM software (COMSOL) was used and some of the most commonly used trajectories for medical applications, micropositioning, micro-object manipulation, etc., were examined. The results showed that the proposed microgripper was capable of generating any parametrizable trajectory. Parametric studies were also carried out by examining the most relevant parameters highlighting their influence on specimen trajectories.

Keywords: MEMS; piezoelectric; path generator

check for updates

Citation: Botta, F. A Piezoelectric MEMS Microgripper for Arbitrary XY Trajectory. *Micromachines* **2022**, *13*, 1888. https://doi.org/10.3390/mi13111888

Academic Editors: Fabio Di Pietrantonio and Stephen Saddow

Received: 22 August 2022
Accepted: 16 September 2022
Published: 1 November 2022

Publisher's Note: MDPI stays neutral with regard to jurisdictional claims in published maps and institutional affiliations.

1. Introduction

Lately MEMS have undergone considerable development because of their applications in many fields: micropositioning [1], micro-object manipulation [2–4], Lab-on-Chip [5], sensors [6], and energy harvesting [7]. In particular, MEMS capable of making a body perform particular 2D trajectories have been used in: biological micro-/nanomanipulation [8,9], scanning probe microscopy based nanoimaging [10,11], micro-opto-electromechanical systems [12], etc. Rather complex mechanisms are typically used in this regard [13–15] or systems using two piezoelectric translator actuators (PEAs) arranged orthogonally in the plane of the desired trajectory [16–18]. In fact, piezoelectric materials due to their high response speed, wide frequency bandwidth, etc., are widely used in precision engineering, soft materials analysis and characterization [19] harvesting, vibration control [20–23], etc. However, PEAs typically cannot produce large displacements (a 10 mm long PZT generally has a stroke of 10 microns [24]), and this results in a frequent need of displacement amplification systems such as flexure hinge-based compliant, Scott Russell [25], Z-shaped [26], bridge-type [16], and rhombic mechanisms, the displacements are amplified up to tens of micrometers [27]. In recent years, these have been used less and less because the use of such complex systems worsens the dynamic and static characteristics of the system by reducing its structural stiffness and intrinsic resonant frequency [27]. In contrast, there are a few studies that directly use the piezoelectric effect on the structure to achieve the desired trajectory [28,29].

In this paper, a new device is proposed that uses a different approach with respect to those described previously. The structure is symmetrical with respect to the x-axis, and on the same axis, the element to be moved is placed. Unlike devices using PEAs, in this case, the actions of piezoelectrics are directly exploited: in fact, piezoelectric plates are used to deform the structure and through this deformation the displacement of the specimen is obtained. Such a structure is, basically, divided into two parts: x-displacement unit and y-displacement units. In the first part, the piezoelectric actions are symmetrical with respect to the x-axis so that the specimen can displace only along that axis, while in the second part they are asymmetrical so that they can displace only along the y-axis. By combining these two actions, any kind of 2D trajectory can be obtained.

The characteristics of the proposed mechanism are the simplicity of its construction (it does not need displacement amplification systems) and its versatility. In fact, in contrast to other mechanisms that directly use the piezoelectric effect on the structure, allowing one to realize only simple trajectories, in this case, all kinds of parametric trajectories can be realized, switching from one to another by simply changing the electrical voltage supplied to the piezoelectric plates. In addition, again by varying the voltage, the working range can be changed from a few microns to tens of microns. Such trajectories can be applied in many fields such as micromanipulation, medical treatments (such as the removal of calcifications and obstructions present on arterial walls), to investigate, at the atomic level, the physical properties of matters, etc. This system could, in the future, take advantage of piezoelectric nanogenerators [30,31] or other power systems [32] to build a self-powered device.

2. Analytical Model

A schematic of the proposed model is shown in Figure 1:

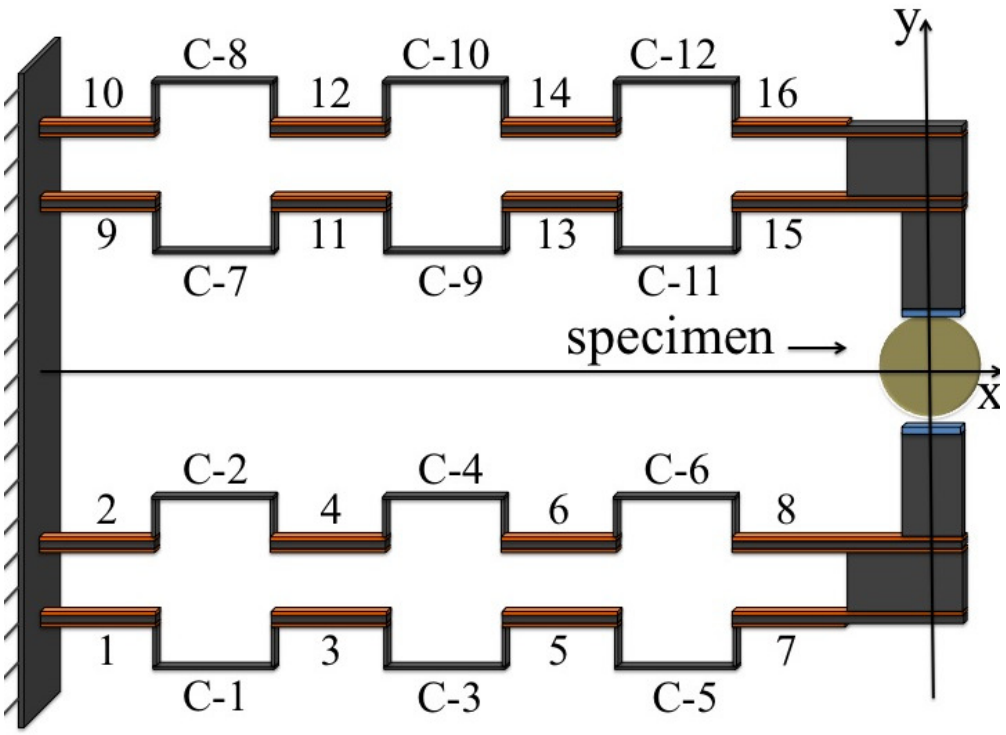

Figure 1. Geometry of the proposed piezoelectric-based MEMS device.

The structure consists of 16 rectilinear beams connected to each other by 12 C-beams; to each rectilinear beam are symmetrically attached two piezoelectric plates (in orange in the figure). The displacement of the specimen is obtained by deforming the structure by means of the action of the piezoelectric plates. In fact, by supplying an electrical voltage to such plates, they will tend to deform (see Figure 2); by bonding them to the beam, this deformation will be partially limited and so they will apply a stress state to the beam. Several studies [33] have shown that this stress state is concentrated at the end of the plates, and the action on the beam can be represented, in essence, by two bending moments $M_a(t)$:

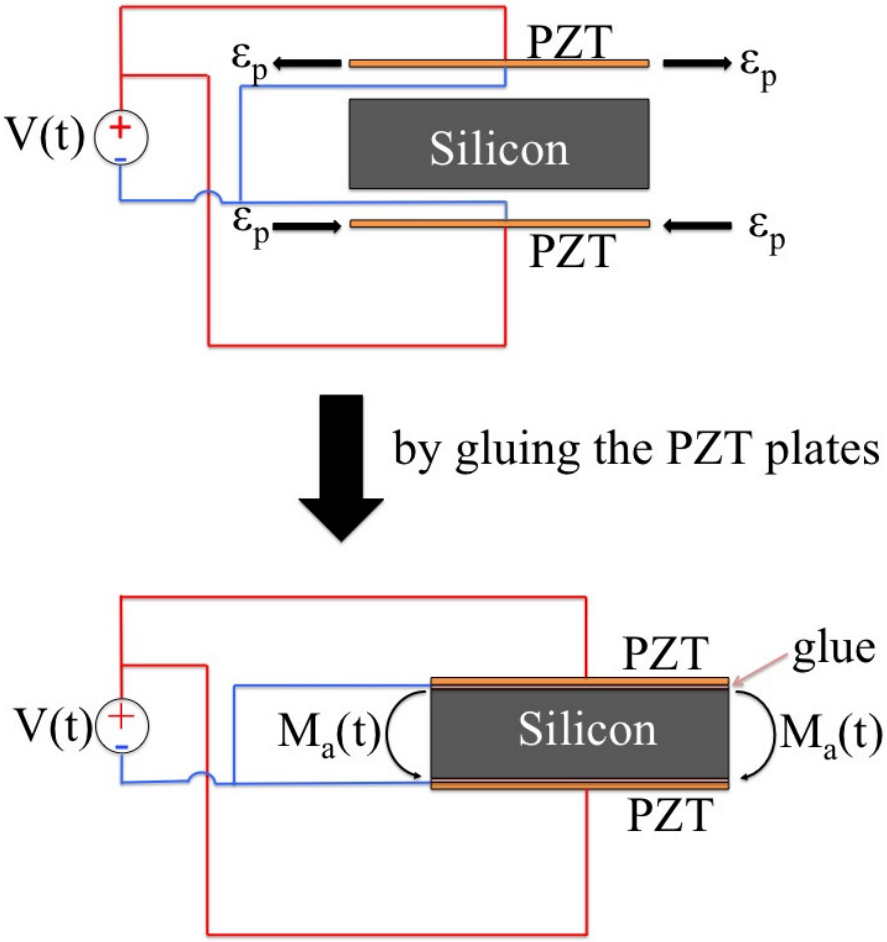

Figure 2. A schematic representation of the pin force model.

where (see [23,33,34]):

$$M_a(t) = \frac{\psi}{6+\psi} E_p b h_p h_M \Lambda(t) \tag{1}$$

and

$$\begin{cases} \psi = \dfrac{E_M h_M}{E_p h_p} \\ \Lambda(t) = \dfrac{d_{31}}{h_p} V(t) \end{cases} \tag{2}$$

The purpose of C-beams is to reduce the axial stiffness of the entire structure by allowing appreciable displacements in that direction. The symmetry of the structure with respect to the x-axis, and the placement of the specimen on the same axis, allows the specimen to move only along this axis when the load applied to the structure is also symmetrical. On the other side, it can move only along the y-axis when that load is asymmetrical. By combining these two actions, the specimen can take any trajectory in the x–y plane. For this purpose, the system was divided into two parts: x displacement unit and y displacement unit (see Figure 3):

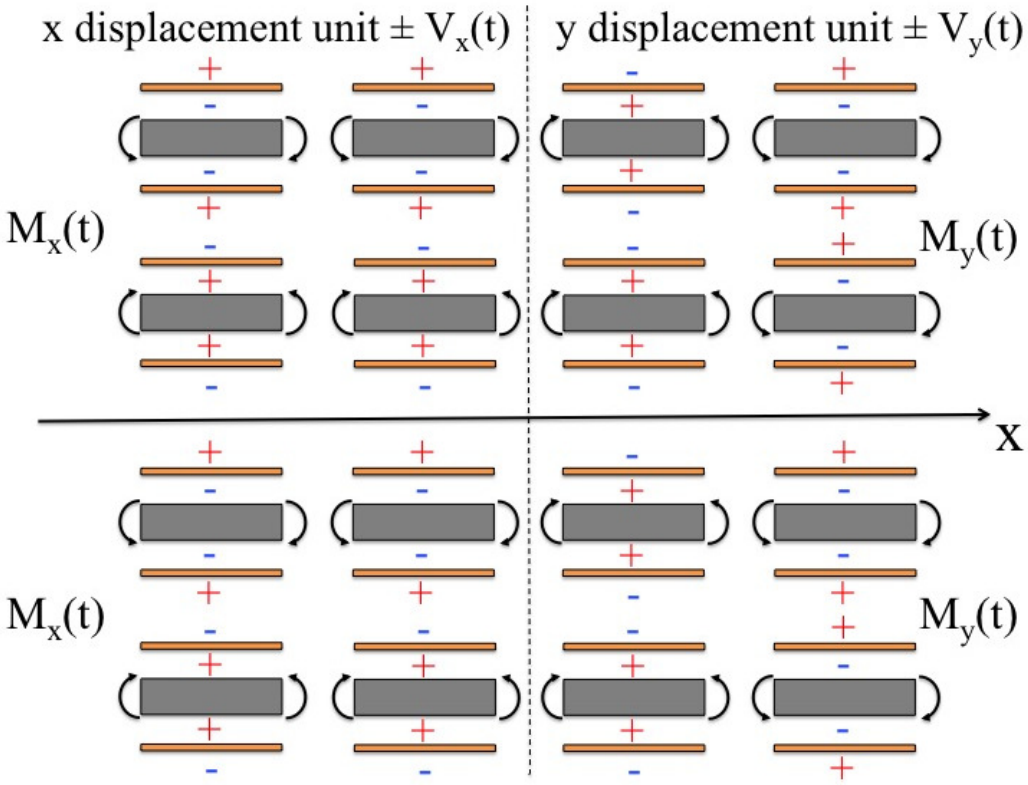

Figure 3. Example of symmetrical and antisymmetrical loads with respect to the x-axis. $M_x(t)$ and $M_y(t)$ denote, respectively, the bending moments which produce only x-axis and y-axis motion of the tip.

The distribution of electrical voltages was such that it provided only symmetrical loads in the first unit and only antisymmetrical loads in the second unit.

The voltage supplying the x-unit was denoted by $V_x(t)$, to which the applied moment $M_x(t)$ corresponds, and the voltage supplying the y-unit, to which the applied moment $M_y(t)$ corresponds, was denoted by $V_y(t)$. Denoting by $u(t)$ and $v(t)$ the displacements of the specimen along the x- and y-axes, the following could be written:

$$\begin{cases} u(t) = B_x M_x(t) \\ v(t) = B_y M_y(t) \end{cases} \tag{3}$$

where the constants B_x and B_y depend on the configuration of the structure, boundary conditions, material properties, etc. Considering (1) and (2), (3) becomes:

$$\begin{cases} u(t) = C_x V_x(t) \\ v(t) = C_y V_y(t) \end{cases} \tag{4}$$

with:

$$\begin{cases} C_x = B_x \dfrac{\psi}{6+\psi} E_p b h_M d_{31} \\ C_y = B_y \dfrac{\psi}{6+\psi} E_p b h_M d_{31} \end{cases} \tag{5}$$

If $x_p(t)$ and $y_p(t)$ represent the parametric equations of the desired trajectory for the specimen, it suffices to pose:

$$\begin{cases} u(t) = x_p(t) \\ v(t) = y_p(t) \end{cases} \tag{6}$$

which, with (4), becomes:

$$\begin{cases} V_x(t) = \dfrac{1}{C_x} x_p(t) \\ V_y(t) = \dfrac{1}{C_y} y_p(t) \end{cases} \tag{7}$$

from which the tensions necessary to execute the desired trajectory can be derived. In this way any trajectory can be achieved.

3. Results and Discussion

A multiphysics FEM software tool (COMSOL) was utilized to verify the proposed microdevice. Typical MEMS material (silicon) was used for the structure while PZT-5A was chosen for the piezoelectric plates. The material properties are given in Table 1.

Table 1. Materials properties.

Property	Silicon	PZT-5A	Unit
Density	2329	7750	kg/m^3
Poisson's ratio	0.28	–	–
Young's modulus	170	–	GPa
$d_{31} = d_{32}$	–	−1.71	10^{-10} C/N
d_{33}	–	3.74	10^{-10} C/N
$d_{51} = d_{42}$	–	5.84	10^{-10} C/N

The details of the geometry and the values of the different quantities are reported in Figure 4 and Table 2:

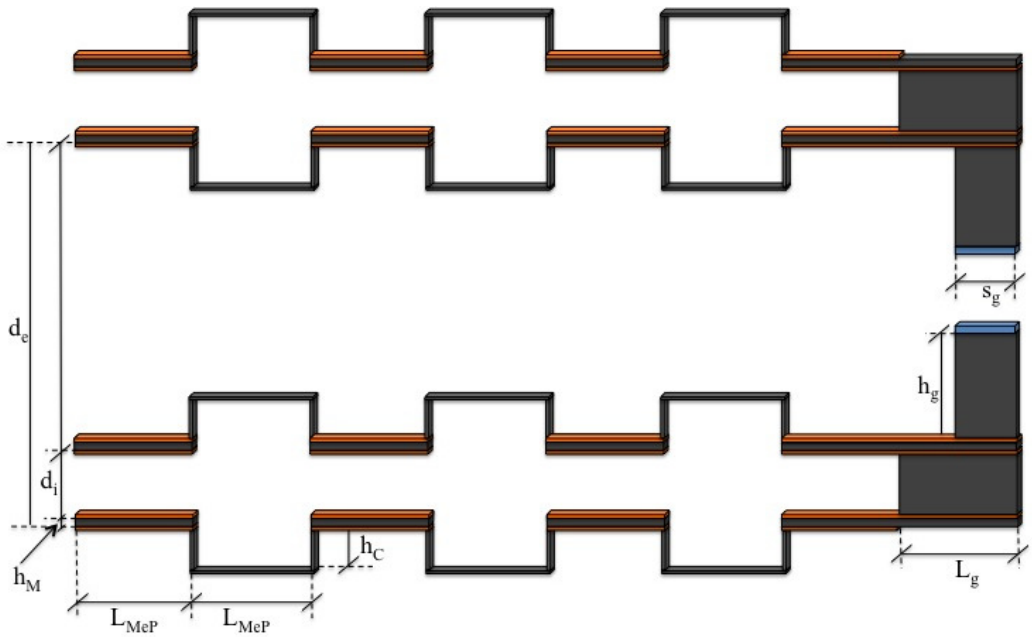

Figure 4. Relevant dimensions of the proposed piezoelectric-based MEMS device.

Table 2. Piezoelectric-based microdevice geometric specifications.

Label	Value (μm)	Label	Value (μm)
L_{MeP}	300	h_M	10
L_g	270	h_C	36
d_i	100	h_g	119
d_e	500	s_g	120
Out-of-plane thickness			10

To test the potential of the proposed model some of the most commonly used trajectories for micro-object manipulation, micropositioning, medical treatment (endoluminal treatment of obstructive lesions, microsurgical operations, arteries unclogging), etc., were examined. The list of trajectories and their electrical voltages used are shown in Table 3.

Table 3. Voltage functions $V_x(t)$ and $V_y(t)$ required to generate the desired pathways.

	Trajectory		Voltage Functions	
Label	$f_x(t)$	$f_y(t)$	$V_x(t)$	$V_y(t)$
Circular	$a\cos(t)$	$a\sin(t)$	$40\cos(t)$	$5.473\sin(t)$
Elliptical	$a\cos(t)$	$b\sin(t)$	$40\cos(t)$	$2\sin(t)$
Straight line	$a\cos(t)$	$b(t)$	$40\cos(t)$	$5.473\sin(t)$
Spiral	$a(e^{\frac{t}{10}}-1)\cos(5t)$	$b(e^{\frac{t}{10}}-1)\sin(5t)$	$40(e^{\frac{t}{10}}-1)\cos(5t)$	$5.473(e^{\frac{t}{10}}-1)\sin(5t)$
Cycloidal	$\frac{a}{2\pi}(t+\sin(10t))$	$b\cos(10t)$	$\frac{40}{2\pi}(t+\sin(10t))$	$3\cos(10t)$
Infinity	$a\sin(t)$	$b\sin(2t)$	$40\sin(t)$	$5.473\sin(2t)$
Star	$a\sin(12t)\cos(t)$	$b\sin(12t)\sin(t)$	$40\sin(12t)\cos(t)$	$5.473\sin(12t)\sin(t)$
Cardioid	$a(2*\cos(t)+\cos(2t))$	$b*(2*\sin(t)+\sin(2t))$	$15(2*\cos(t)+\cos(2t))$	$2*(2*\sin(t)+\sin(2t))$
Nephroid	$a(4*\cos(t)+\cos(4t))$	$b*(4*\sin(t)+\sin(4t))$	$7.5(4*\cos(t)+\cos(4t))$	$1*(4*\sin(t)+\sin(4t))$
Four-leaf clover	$a\sin(2t)\cos(t)$	$b\sin(2t)\sin(t)$	$40\sin(2t)\cos(t)$	$5.473\sin(2t)\sin(t)$
Lissajous 1	$a\sin(2t)$	$b\sin(3t)$	$40\sin(2t)$	$5.473\sin(3t)$
Lissajous 2	$a\sin(10t)$	$b\sin(7t)$	$40\sin(10t)$	$5.473\sin(7t)$

The results are shown in Figures 5 and 6. They show that the mechanism was able to follow all set trajectories. Only in some cases was there a small initial oscillation due to the fact that the mechanism always started from the origin and if the initial point of the trajectory was not at the origin there was an initial *"step"* that resulted in such oscillations. However, these were quickly damped and then the mechanism followed the set trajectory.

In order to verify that the stresses did not exceed the maximum allowable value, the Von Mises stress plots are shown for some trajectories in the most severe situations (Figure 7). It can be observed that the stresses never exceeded 2 GPa, well within the preyield stress.

The working space could be changed, for each trajectory, simply by varying the amplitude of the electrical voltage supplied to the piezoelectric plates. Figure 8 shows some results in which the same type of trajectories were obtained with different voltages. It can be seen that the mechanism was able to go from a few microns to hundreds of microns.

The effects of the geometrical dimensions on the amplitude of the trajectories were also investigated. They were different, in accordance with the type of parameter being considered. The first to be examined see Figures 9 and 10 was the height of the connecting C-structure between the straight beams (h_C in Figure 4).

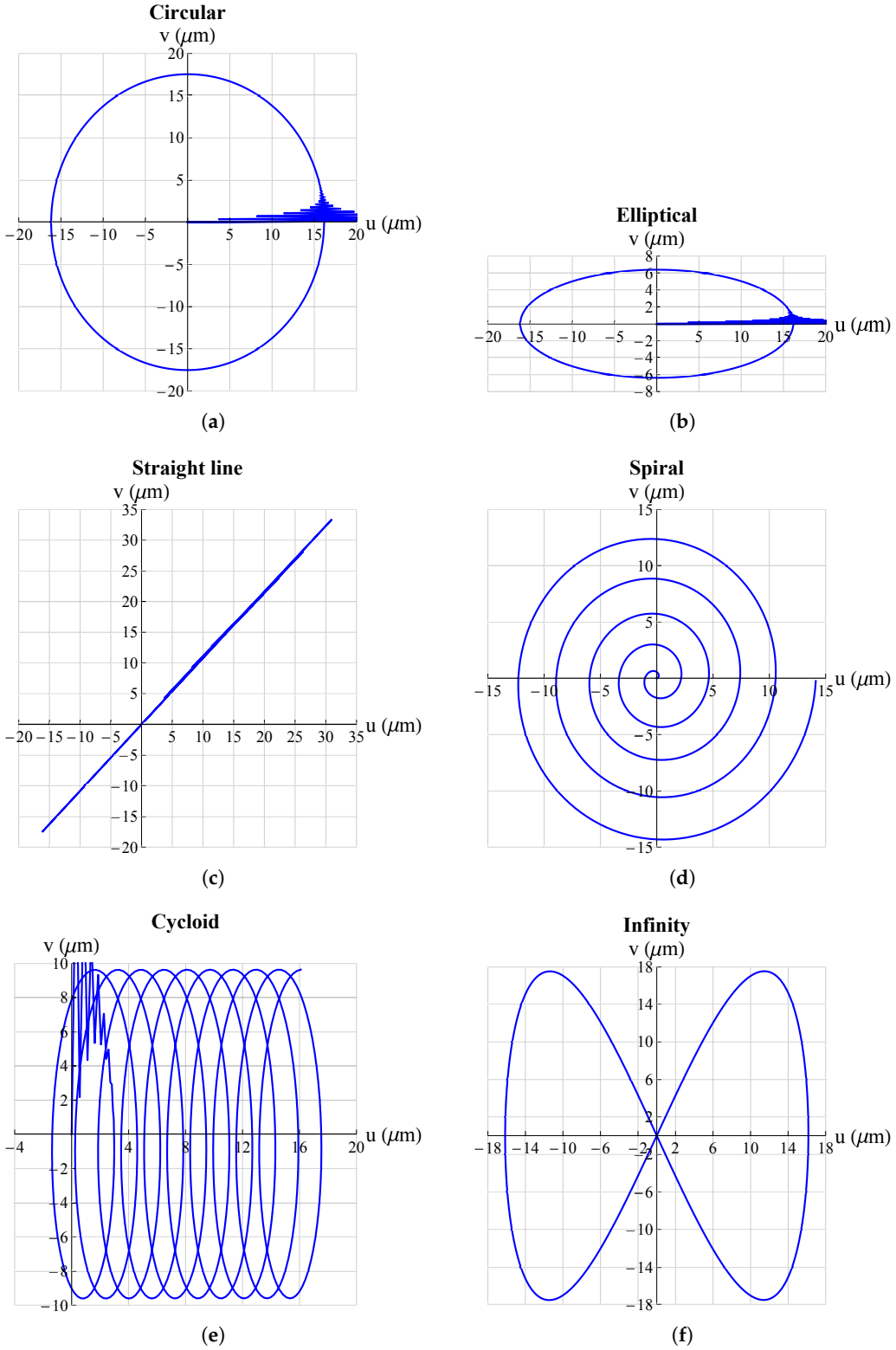

Figure 5. Some possible trajectories applicable, just to mention a few examples, in the medical field for atherectomy operations: (**a**) circular; (**b**) elliptical; (**c**) straight line; (**d**) spiral; (**e**) cycloid; (**f**) infinity. All graphs were obtained by means of FEM simulations.

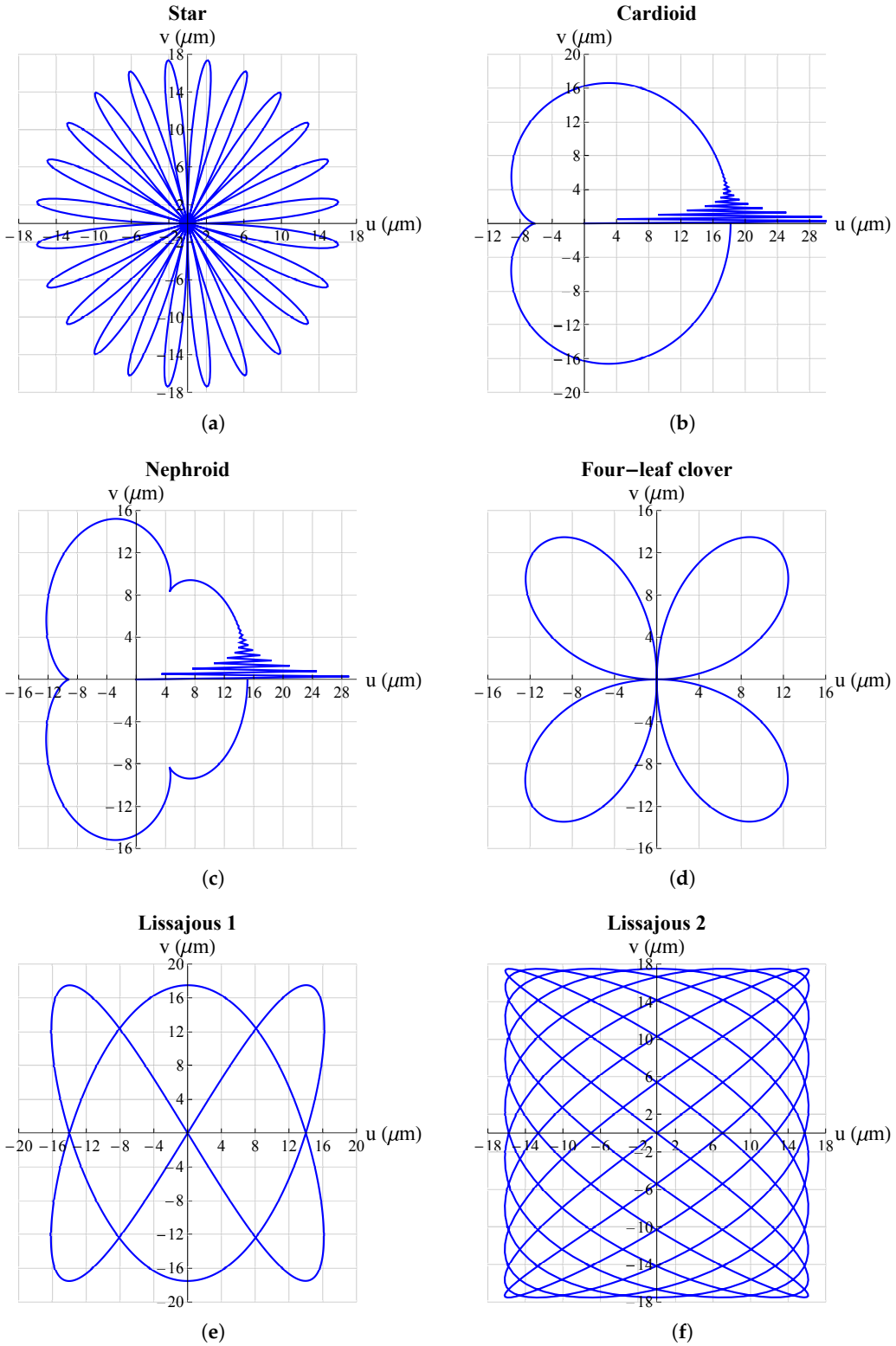

Figure 6. Some possible trajectories applicable, just to mention a few examples, for scanning methods in atomic force microscopes (AFM): (**a**) star; (**b**) cardioid; (**c**) nephroid; (**d**) four-leaf clover; (**e**) Lisaajous-1; (**f**) Lissajous 2. All graphs were obtained by means of FEM simulations.

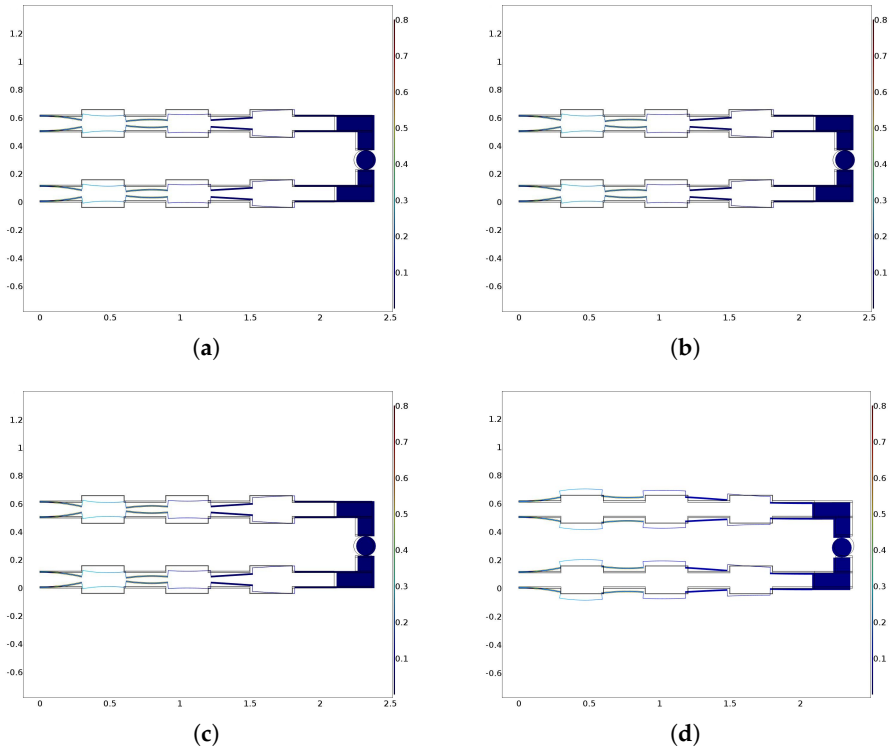

Figure 7. Von Mises stress for (**a**) circular, (**b**) elliptical, (**c**) cycloidal, and (**d**) Lissajous 1 trajectories. All graphs were obtained by means of FEM simulations. Stress scale is in GPa.

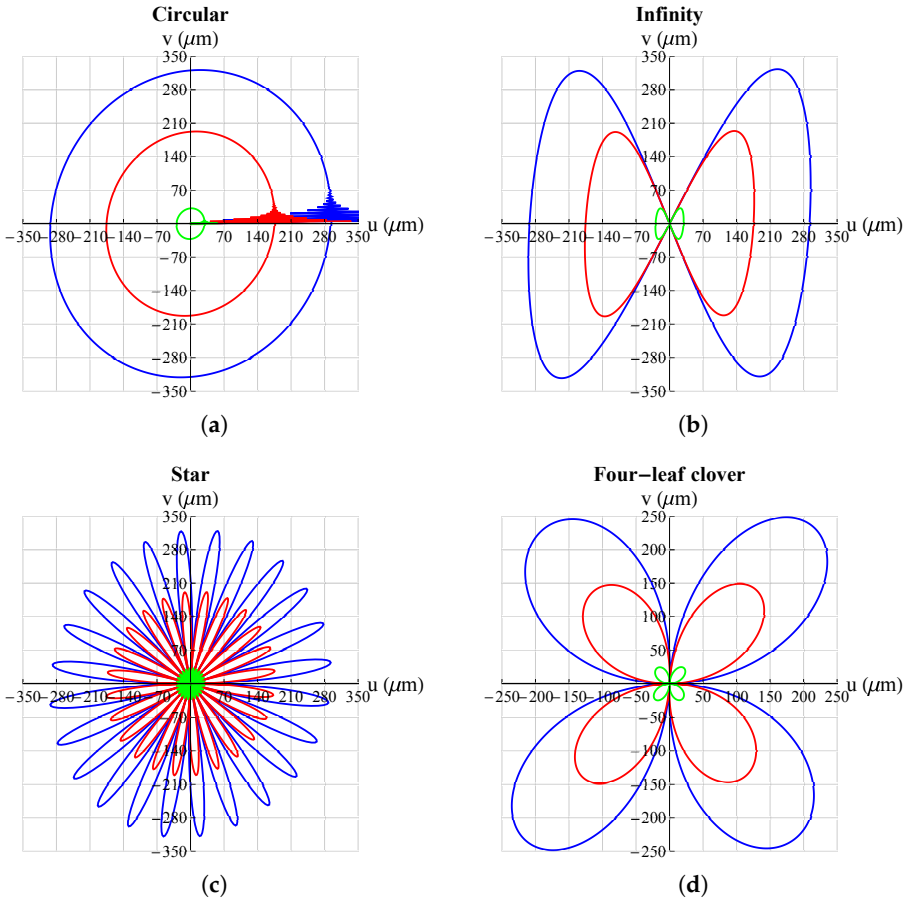

Figure 8. *Cont.*

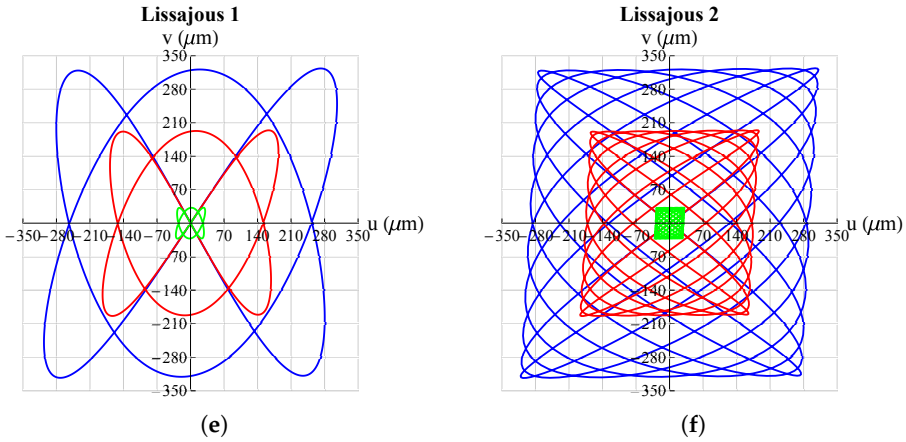

Figure 8. Effect of the electrical voltage supplied to piezoelectric plates on different trajectories. _____: $\{V_x = 50$ V, $V_y = 20$ V$\}$; _____: $\{V_x = 30$ V, $V_y = 12$ V$\}$; _____: $\{V_x = 5$ V, $V_y = 2$ V$\}$: (**a**) circular; (**b**) infinity; (**c**) star; (**d**) four-leaf clover; (**e**) Lissajous 1; (**f**) Lissajous 2. All graphs were obtained by means of FEM simulations.

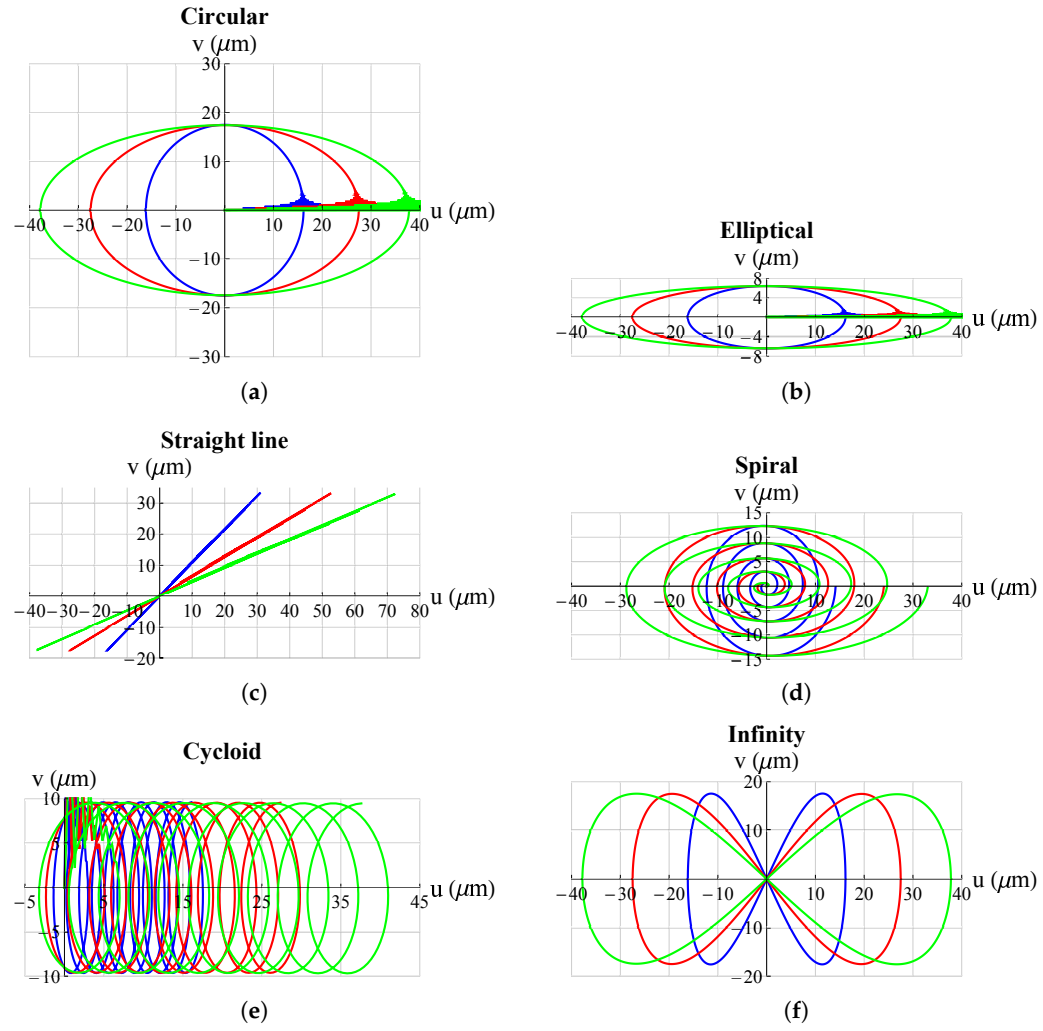

Figure 9. Effect of dimension h_C on different trajectories. _____: $h_C = 36$ μm, _____: $h_C = 72$ μm, _____: $h_C = 108$ μm: (**a**) circular; (**b**) elliptical; (**c**) straight line; (**d**) spiral; (**e**) cycloid; (**f**) infinity. All graphs were obtained by means of FEM simulations.

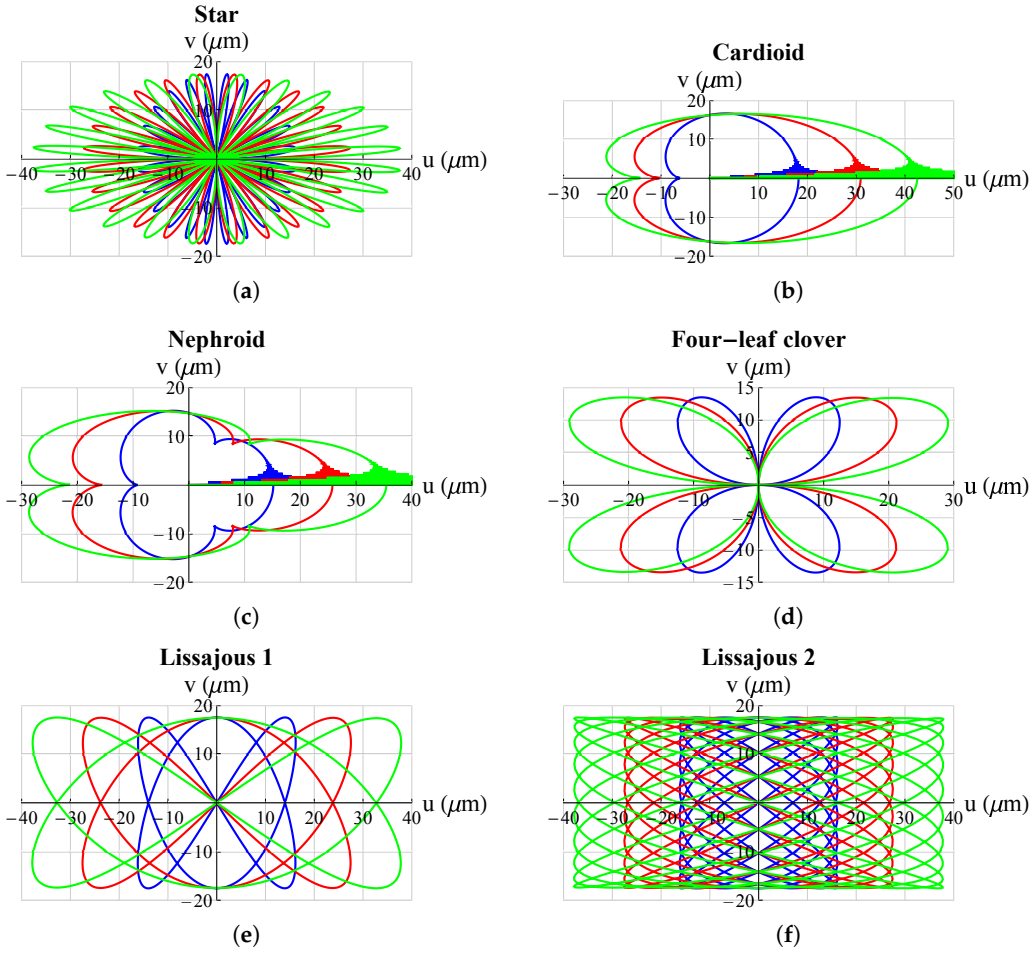

Figure 10. Effect of dimension h_C on different trajectories. _____: $h_C = 36$ μm, _____: $h_C = 72$ μm, _____: $h_C = 108$ μm: (**a**) star; (**b**) cardioid; (**c**) nephroid; (**d**) four-leaf clover; (**e**) Lisaajous-1; (**f**) Lissajous 2. All graphs were obtained by means of FEM simulations.

From the analysis of the figures, it can be seen that h_C had an effect only on the excursion in the x-direction and not in the y-direction or, in other words, this parameter essentially affected only the stiffness of the structure in the x-direction. Moreover, these variations did not depend on the type of trajectory; the results are summarized in Figure 11:

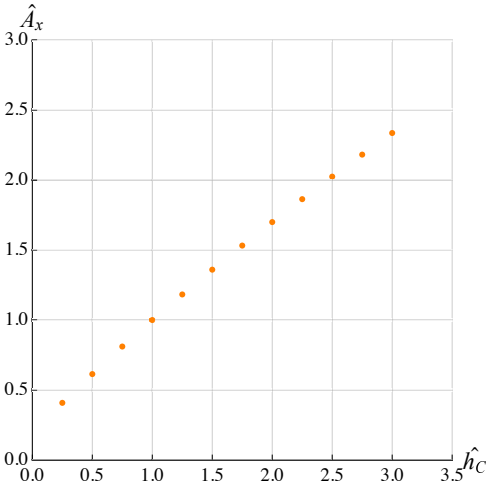

Figure 11. Effect of dimension h_C on $\hat{A}_x$.

where $\hat{h_C}$ is the dimensionless value of h_C with respect to the chosen reference value present in Table 2 and $\hat{A_x}$ is the amplitude variation with respect to the reference amplitude. It can be observed that the variation is linear.

The second parameter examined was L_{MeP}. The results are shown in Figure 12 (by way of illustration, not all cases are reported but only some simulations).

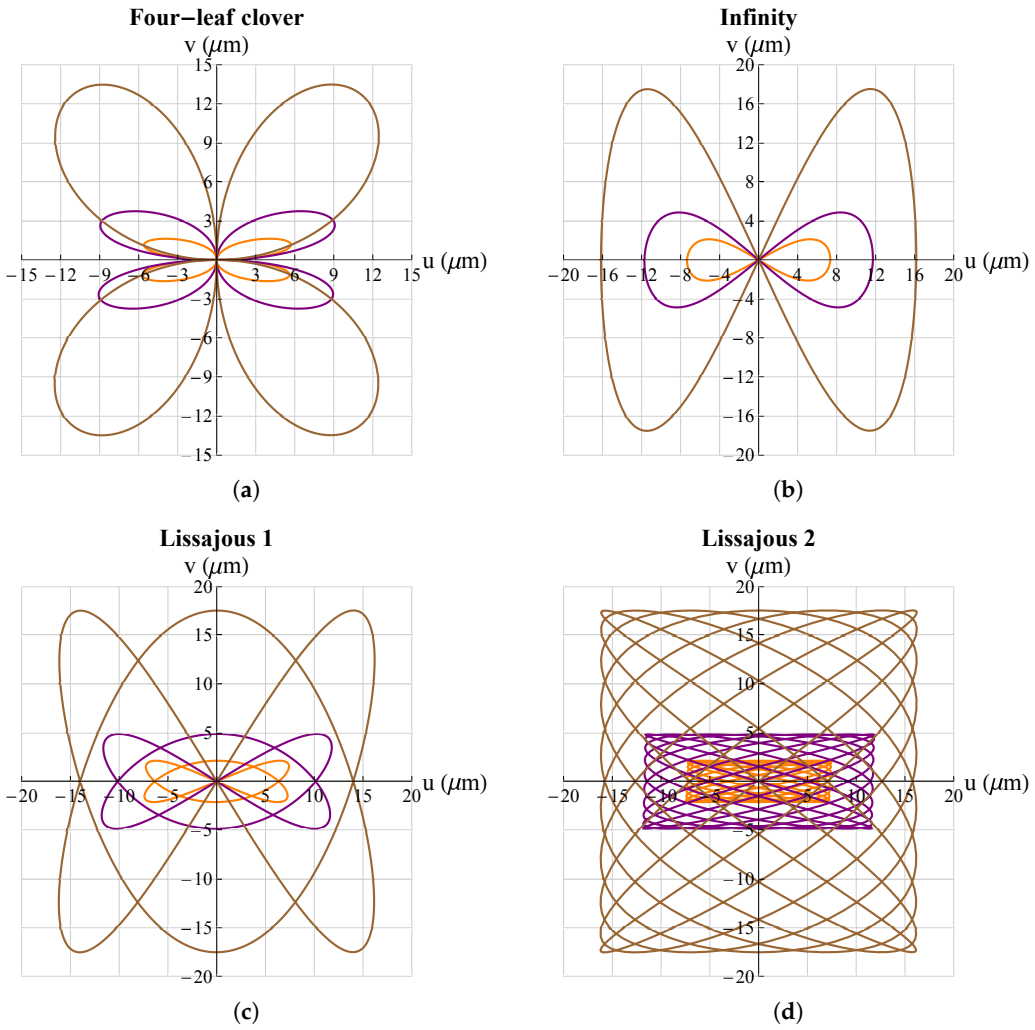

Figure 12. Effect of dimension L_{MeP} on different trajectories. _____: L_{MeP} = 300 µm, _____: L_{MeP} = 225 µm, _____: L_{MeP} = 150 µm: (**a**) four-leaf clover; (**b**) infinity; (**c**) Lissajous 1; (**d**) Lissajous 2. All graphs were obtained by means of FEM simulations.

In this case, it can be seen that the parameter impacted the amplitude of the working range on both the *x*- and *y*-axes; however, this effect was more pronounced on the *y*-axis than on the *x*-axis. In order to highlight these changes, a graph summarizing the results obtained are shown in Figure 13.

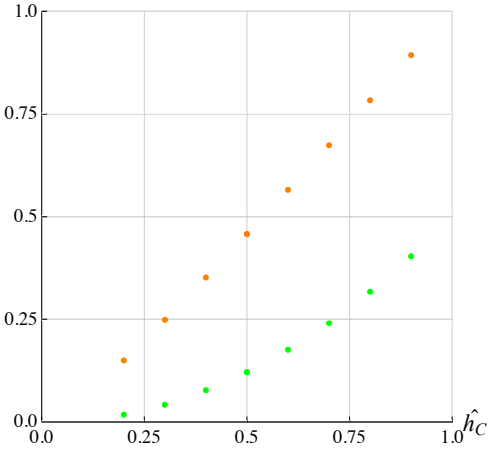

Figure 13. Effect of dimension L_{MeP} on $\hat{A}_x$ (in orange) and $\hat{A}_y$ (in green).

Finally, the effect of the MEMS thickness h_M was studied (Figure 14).

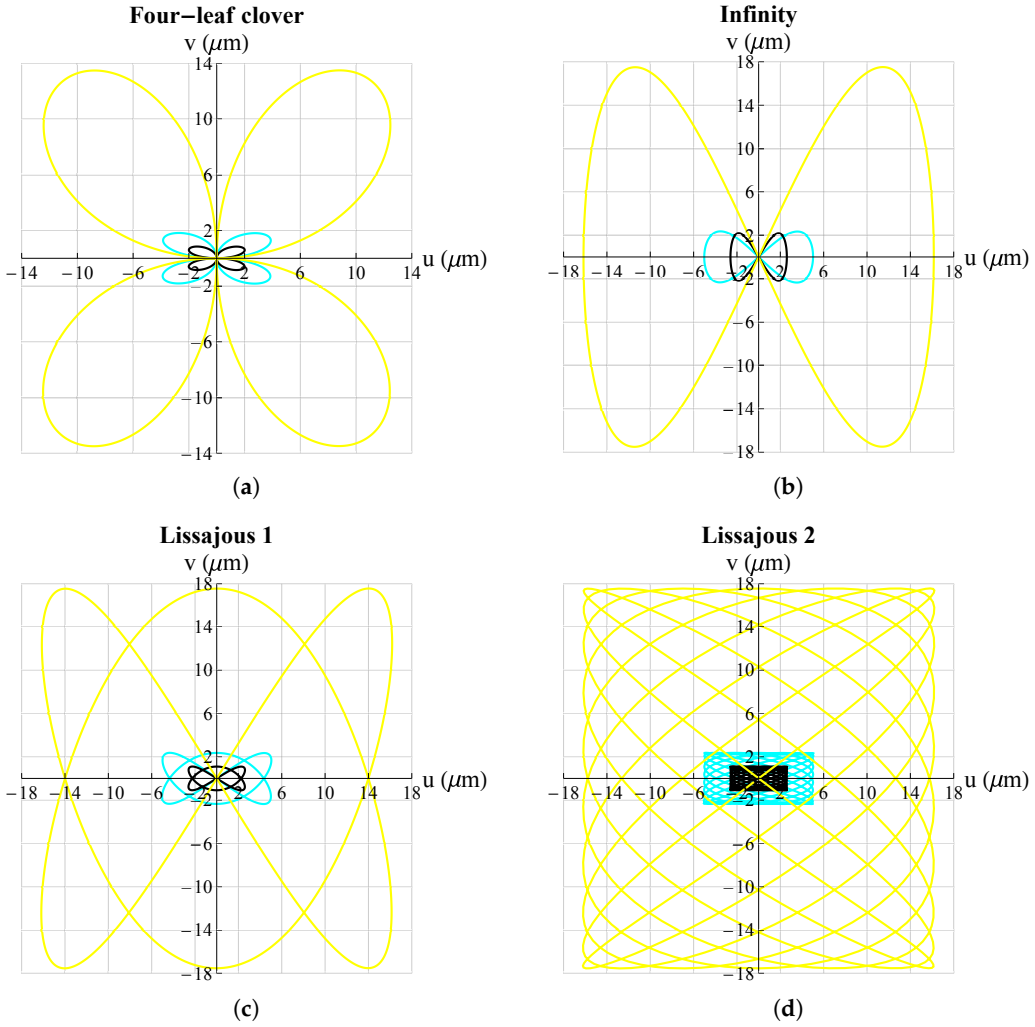

Figure 14. Effect of dimension h_M on different trajectories. _____: h_M = 10 µm, _____: h_M = 20 µm, _____: h_M = 30 µm: (**a**) four-leaf clover; (**b**) infinity; (**c**) Lissajous 1; (**d**) Lissajous 2. All graphs were obtained by means of FEM simulations.

From the figure it can be seen that h_M also affected the working range on both axes but this time, the effect seemed essentially of the same type; in Figure 15 the results obtained for the cloverleaf trajectory are shown.

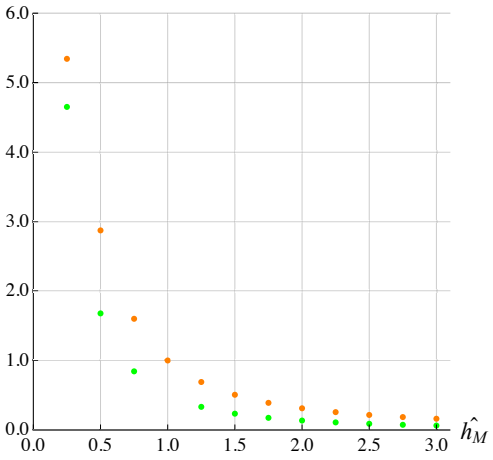

Figure 15. Effect of dimension h_M on $\hat{A}_x$ (in orange) and $\hat{A}_y$ (in green).

4. Conclusions

A new microgripper was proposed. The grasping and displacement of the specimen was accomplished by deforming a symmetrical structure through the action of piezoelectric plates. It was shown that the proposed system was capable of performing any type of plane parametric trajectory with a displacement head ranging from a few microns to hundreds of microns simply by acting on the voltage that was supplied to the piezoelectric plates. A parametric study was also conducted to highlight the effect of certain geometrical characteristics of the structure on the amplitude of the trajectories.

Funding: This research received no external funding.

Conflicts of Interest: The author declares no conflict of interest.

Nomenclature

b	out of plane thickness
E_M	Young's modulus of silicon
E_p	Young's modulus of PZT
h_M	thickness of silicon
h_P	thickness of PZT
M_a	bending moment applied by PZTs
u	displacement of the specimen along the x-axis
v	displacement of the specimen along the y-axis
V_x, V_y	electrical voltages supplied to PZTs
$x_p(t), y_p(t)$	parametric equations of the wanted trajectory

References

1. Dong, J.; Mukhopadhyay, D.; Ferreira, P.M. Design, fabrication and testing of a silicon-on-insulator (SOI) MEMS parallel kinematics XY stage. *J. Micromech. Microeng.* **2007**, *17*, 1154–1161. [CrossRef]
2. Botta, F.; Verotti, M.; Bagolini, A.; Bellutti, P.; Belfiore, N.P. Mechanical response of four-bar linkage microgrippers with bidirectional electrostatic actuation. *Actuators* **2018**, *7*, 78. [CrossRef]
3. Otic, C.J.C.; Yonemura, S. Thermally Induced Knudsen Forces for Contactless Manipulation of a Micro-Object. *Micromachines* **2022**, *13*, 1092. [CrossRef] [PubMed]
4. Zhao, Y.; Huang, X.; Liu, Y.; Wang, G.; Hong, K. Design and Control of a Piezoelectric-Driven Microgripper Perceiving Displacement and Gripping Force. *Micromachines* **2020**, *11*, 121. [CrossRef]
5. Dawson, H.; Elias, J.; Etienne, P.; Calas-Etienne, S. The Rise of the OM-LoC: Opto-Microfluidic Enabled Lab-on-Chip. *Micromachines* **2021**, *12*, 1467. [CrossRef] [PubMed]

6. Zhu, H.; Zheng, F.; Leng, H.; Zhang, C.; Luo, K.; Cao, Y.; Yang, X. Simplified Method of Microcontact Force Measurement by Using Micropressure Sensor. *Micromachines* **2021**, *12*, 515. [CrossRef]
7. Tian, W.; Ling, Z.; Yu, W.; Shi, J. A Review of MEMS Scale Piezoelectric Energy Harvester. *Appl. Sci.* **2018**, *8*, 645. [CrossRef]
8. Gu, G.Y.; Zhu, L.M.; Su, C.Y.; Ding, H.; Fatikow, S. Modeling and control of piezo-actuated nanopositioning stages: A survey. *IEEE Trans. Autom. Sci. Eng.* **2014**, *13*, 313–332. [CrossRef]
9. Li, Y.; Xu, Q. Design and analysis of a totally decoupled flexure-based XY parallel micromanipulator. *IEEE Trans. Robot.* **2009**, *25*, 645–657.
10. Zhu, W.L.; Zhu, Z.; Shi, Y.; Wang, X.; Guan, K.; Ju, B.F. Design, modeling, analysis and testing of a novel piezo-actuated XY compliant mechanism for large workspace nano-positioning. *Smart Mater. Struct.* **2016**, *25*, 115033. [CrossRef]
11. Yong, Y.K.; Aphale, S.S.; Moheimani, S.R. Design, identification, and control of a flexure-based XY stage for fast nanoscale positioning. *IEEE Trans. Nanotechnol.* **2008**, *8*, 46–54. [CrossRef]
12. Laszczyk, K.; Bargiel, S.; Gorecki, C.; Krężel, J.; Dziuban, P.; Kujawińska, M.; Callet, D.; Frank, S. A two directional electrostatic comb-drive X–Y micro-stage for MOEMS applications. *Sens. Actuators A Phys.* **2010**, *163*, 255–265. [CrossRef]
13. Lin, C.; Shen, Z.; Wu, Z.; Yu, J. Kinematic characteristic analysis of a micro-/nano positioning stage based on bridge-type amplifier. *Sens. Actuators A Phys.* **2018**, *271*, 230–242. [CrossRef]
14. Zubir, M.N.M.; Shirinzadeh, B.; Tian, Y. Development of a novel flexure-based microgripper for high precision micro-object manipulation. *Sens. Actuators A Phys.* **2009**, *150*, 257–266. [CrossRef]
15. Yao, Q.; Dong, J.; Ferreira, P.M. Design, analysis, fabrication and testing of a parallel-kinematic micropositioning XY stage. *Int. J. Mach. Tools Manuf.* **2007**, *47*, 946–961. [CrossRef]
16. Zhou, M.; Fan, Z.; Ma, Z.; Zhao, H.; Guo, Y.; Hong, K.; Li, Y.; Liu, H.; Wu, D. Design and experimental research of a novel stick-slip type piezoelectric actuator. *Micromachines* **2017**, *8*, 150. [CrossRef]
17. Chen, X.; Li, Y. Design and analysis of a new high precision decoupled XY compact parallel micromanipulator. *Micromachines* **2017**, *8*, 82. [CrossRef]
18. Pang, J.; Liu, P.; Yan, P.; Zhang, Z. Modeling and experimental testing of a composite bridge type amplifier based nano-positioner. In Proceedings of the 2016 IEEE International Conference on Manipulation, Manufacturing and Measurement on the Nanoscale (3M-NANO), Chongqing, China, 18–22 July 2016; pp. 25–30.
19. Botta, F.; Rossi, A.; Belfiore, N.P. A feasibility study of a novel piezo MEMS tweezer for soft materials characterization. *Appl. Sci.* **2019**, *9*, 2277. [CrossRef]
20. Botta, F.; Rossi, A.; Belfiore, N.P. A novel method to fully suppress single and bi-modal excitations due to the support vibration by means of piezoelectric actuators. *J. Sound Vib.* **2021**, *510*, 116260. [CrossRef]
21. Botta, F.; Marx, N.; Gentili, S.; Schwingshackl, C.; Di Mare, L.; Cerri, G.; Dini, D. Optimal placement of piezoelectric plates for active vibration control of gas turbine blades: Experimental results. In *Sensors and Smart Structures Technologies for Civil, Mechanical, and Aerospace Systems*; SPIE: San Diego, CA, USA, 2012; Volume 8345, pp. 655–665.
22. Botta, F.; Marx, N.; Schwingshackl, C.; Cerri, G.; Dini, D. A wireless vibration control technique for gas turbine blades using piezoelectric plates and contactless energy transfer. In *Turbo Expo: Power for Land, Sea, and Air*; American Society of Mechanical Engineers: San Antonio, TX, USA, 2013; Volume 55263, p. V07AT32A006.
23. Botta, F.; Scorza, A.; Rossi, A. Optimal Piezoelectric Potential Distribution for Controlling Multimode Vibrations. *Appl. Sci.* **2018**, *8*, 551. [CrossRef]
24. Shimizu, Y.; Peng, Y.; Kaneko, J.; Azuma, T.; Ito, S.; Gao, W.; Lu, T.F. Design and construction of the motion mechanism of an XY micro-stage for precision positioning. *Sens. Actuators A Phys.* **2013**, *201*, 395–406. [CrossRef]
25. Ai, W.; Xu, Q. New Structural Design of a Compliant Gripper Based on the Scott-Russell Mechanism. *Int. J. Adv. Robot. Syst.* **2014**, *11*, 192. [CrossRef]
26. Li, J.; Liu, H.; Zhao, H. A compact 2-DOF piezoelectric-driven platform based on "z-shaped" flexure hinges. *Micromachines* **2017**, *8*, 245. [CrossRef]
27. Zhang, L.; Huang, H. *Parasitic Motion Principle (PMP) Piezoelectric Actuators: Definition and Recent Developments*; IntechOpen: London, UK, 2021.
28. DeVoe, D.L.; Pisano, A.P. Modeling and optimal design of piezoelectric cantilever microactuators. *J. Microelectromech. Syst.* **1997**, *6*, 266–270. [CrossRef]
29. El-Sayed, A.M.; Abo-Ismail, A.; El-Melegy, M.T.; Hamzaid, N.A.; Abu Osman, N.A. Development of a micro-gripper using piezoelectric bimorphs. *Sensors* **2013**, *13*, 5826–5840. [CrossRef]
30. Sahoo, S.; Ratha, S.; Rout, C.S.; Nayak, S.K. Self-charging supercapacitors for smart electronic devices: A concise review on the recent trends and future sustainability. *J. Mater. Sci.* **2022**, *57*, 4399–4440. [CrossRef]
31. Aaryashree; Sahoo, S.; Walke, P.; Nayak, S.K.; Rout, C.S.; Late, D.J. Recent developments in self-powered smart chemical sensors for wearable electronics. *Nano Res.* **2021**, *14*, 3669–3689. [CrossRef]
32. Sahoo, S.; Krishnamoorthy, K.; Pazhamalai, P.; Mariappan, V.K.; Manoharan, S.; Kim, S.J. High performance self-charging supercapacitors using a porous PVDF-ionic liquid electrolyte sandwiched between two-dimensional graphene electrodes. *J. Mater. Chem. A* **2019**, *7*, 21693–21703. [CrossRef]
33. Crawley, E.F.; de Luis, J. Use of piezoelectric actuators as elements of intelligent structures. *AIAA J.* **1987**, *25*, 1373–1385. [CrossRef]
34. Botta, F.; Toccaceli, F. Piezoelectric plates distribution for active control of torsional vibrations. *Actuators* **2018**, *7*, 23. [CrossRef]